Dianthracenylazatrioxa[8]circulene: synthesis, characterization and application in OLEDs

Pedersen, Stephan K.

2021-08-11

Pedersen , S K , Pedersen , V B , Kamounah , F S , Broløs , L M , Baryshnikov , G V , Valiev , R R , Ivaniuk , K , Stakhira , P , Minaev , B , Karaush-Karmazin , N , Ågren , H & Pittelkow , M 2021 , ' Dianthracenylazatrioxa[8]circulene: synthesis, characterization and application in OLEDs ' , Chemistry: A European Journal , vol. 27 , no. 45 , pp. 11609-11617 . https://doi.org/10.1002/chem.202100

http://hdl.handle.net/10138/343016
https://doi.org/10.1002/chem.202100090

acceptedVersion

Chemistry
A European
Journal

Chemistry Europe
European Chemical Societies Publishing

Accepted Article

Title: Dianthracenylazatrioxa[8]circulene: synthesis, characterization and application in OLEDs

Authors: Stephan K. Pedersen, Viktor B. Pedersen, Fadhil S. Kamounah, Line M. Broløs, Glib V. Baryshnikov, Rashid R. Valiev, Khrystyna Ivaniuk, Pavlo Stakhira, Nataliya Karaush-Karmazin, Boris Minaev, Hans Ågren, and Michael Pittelkow

To be cited as: *Chem. Eur. J.* 10.1002/chem.202100090

Link to VoR: https://doi.org/10.1002/chem.202100090

WILEY-VCH

10.1002/chem.202100090

WILEY-VCH

COMMUNICATION

Dianthracenylazatrioxa[8]circulene: Synthesis, Characterization and Application in OLEDs

Dr. Stephan K. Pedersen,[a] Viktor B. Pedersen,[a] Dr. Fadhil S. Kamounah,[a] Line M. Broløs,[a] Prof. Glib V. Baryshnikov,[b,c,*] Dr. Rashid R. Valiev,[c,d] Dr. Khrystyna Ivaniuk,[e] Prof. Pavlo Stakhira,[e] Prof. Boris Minaev,[f] Dr. Nataliya Karaush-Karmazin,[f] Prof. Hans Ågren,[b,g] and Prof. Michael Pittelkow[a*]

Dedicated to Prof. Jørn Bolstad Christensen on the occasion of his 60th birthday

[a]Department of Chemistry, University of Copenhagen, Universitetsparken 5, DK-2100 Copenhagen Ø, Denmark. E-mail: pittel@chem.ku.dk
[b]Division of Theoretical Chemistry and Biology, School of Engineering Sciences in Chemistry, Biotechnology and Health, KTH Royal Institute of Technology, 10691, Stockholm, Sweden. E-mail: glibar@kth.se
[c]Tomsk State University, 36 Lenin Avenue, Tomsk 634050, Russia
[d]University of Helsinki, Department of Chemistry, P.O. Box 55 (A.I. Virtanens plats 1), FIN-00014 University of Helsinki, Finland
[e]Lviv Polytechnic National University, S. Bandera 12, 79013 Lviv, Ukraine
[f]Department of Chemistry and Nanomaterials Science, Bohdan Khmelnytsky National University, 18031, Cherkasy, Ukraine.
[g]College of Chemistry and Chemical Engineering, Henan University, Kaifeng, Henan 475004, P.R. China

Supporting information for this article is given via a link at the end of the document.

Abstract: A soluble and green-blue fluorescent π-extended azatrioxa[8]circulene was synthesized by oxidative condensation of a 3,6-dihydroxycarbazole and 1,4-anthraquinone utilizing benzofuran scaffolding. This is the first circulene to incorporate anthracene within it carbon framework. Solvent-dependent fluorescence and bright green electroluminescence accompanied by excimer emission are key optical properties of this material. The presence of sliding π-stacked columns in the single crystal of dianthracenylazatrioxa[8]circulene is found to cause a very high rate for the electron hopping making this material a promising n-type organic semiconductor with an electron mobility predicted around 2.26 $cm^2 V^{-1} s^{-1}$. The best OLED device based on the dianthracenylazatrioxa[8]circulene fluorescent emitter has a brightness around 16 000 Cd m^{-2} and external quantum efficiency of 3.3%. By using dianthracenylazatrioxa[8]circulene as a host matrix material the quantum dots based OLEDs were fabricated.

Introduction

The development of new molecules and materials that function as blue-emitting components in organic light emitting diodes (OLEDs) continues to be a challenge both in materials science and in organic chemistry.[1] Any molecular design of an emitter must take into account a range of parameters including chemical stability, solubility, aggregation and colour purity.[2] Certain molecular entities are known to impart blue fluorescence including selected polycyclic aromatic hydrocarbons (PAHs) such as anthracene and chrysene and a range of molecular architectures featuring carbazole units.[3]

In recent work we prepared and studied azatrioxa[8]circulene **3**, which contains carbazole motif, as a promising emitter for blue OLEDs (Figure 1).[4] Hetero[8]circulenes are polyaromatic macrocycles containing five- and six-membered rings surrounding an eight-membered carbon core, i.e. a cyclooctatetraene.[5] Depending on the type and number of heteroatoms in the outer perimeter, these systems may possess planar or saddle-shaped structure [6] as regulated by the Wynberg-Dopper structural model.[7] An extension of the π-electron system of planar circulenes usually leads to an improvement of the light harvesting properties and fluorescence efficiency by these compounds.[8] For example, symmetrical tetraoxa[8]circulene **1** exhibits a very small fluorescence quantum yield (FQY less than 10%),[9a] while the substitution of one or two oxygen atoms by NH groups gives a threefold improvement of the fluorescent efficiency (FQY of circulene **2** and related system with two oppositely arranged NH groups is about 30%).[9b,c]

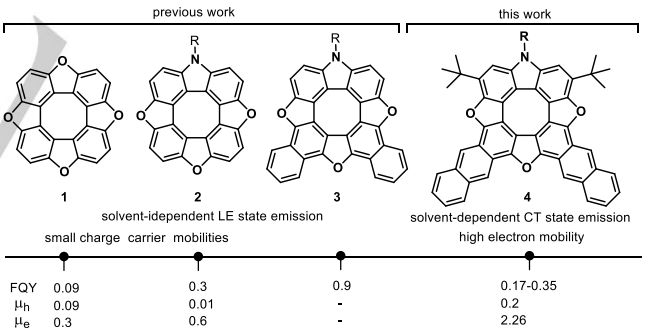

Figure 1. Trend in fluorescence quantum yield (FQY), hole (μ_h) and electron (μ_e) mobility upon O/NH substitution and next π-extension of the circulene skeleton (R = *n*-Pr).

The next extension of the π-system by introducing two naphthyl groups giving **3**, significantly increases the FQY to near unity (~90%).[9c] This strategy was successfully utilized upon the fabrication of efficient green-blue light-emitting diodes based on naphthyl-containing azatrioxa[8]circulenes.[10]

To appreciate the complexity of extending the π-system of azatrioxa[8]circulenes further it is important to understand how the heterocyclic [8]circulenes are synthesized (Figure 2). The earliest heterocyclic [8]circulenes were prepared by Erdtman and Högberg by an acid-mediated tetramerization of benzoquinone to yield the tetraoxa[8]circulene.[11] It was found that benzoquinones with substituents in the 2- and 3-positions yielded more of the circulene structures, and using 1,4-naphthoquinone yielded the corresponding tetraoxa[8]circulene in 90% yield.[11a] We realized

10.1002/chem.202100090

that a key intermediate in the synthesis of tetraoxa[8]circulene is a di-hydroxy-dibenzofuran, which originate from a dimerization of the 1,4-benzoquinone. We extended this concept to yield nitrogen-containing [8]circulenes by replacing this di-hydroxy-dibenzofuran with a di-hydroxy-carbazole. By doing this it is possible to prepare heterocyclic [8]circulenes with either one or two nitrogens. The substrates with one nitrogen was prepared by condensing the di-hydroxy-carbazole with two molecules of a benzoquinone (or naphthoquinone) and the substrates with two nitrogen atoms incorporated were prepared by dimerizing the di-hydroxy-carbazole. The dimerization is an oxidative dimerization, and since quinones are oxidizing agents, the dimerization reaction accompany the formation of the azatrioxa[8]circulene (Figure 2). The dimerization generally works well using a benzoquinone that does not itself incorporate into the heterocyclic [8]circulene scaffold, such as DDQ and chloranil.

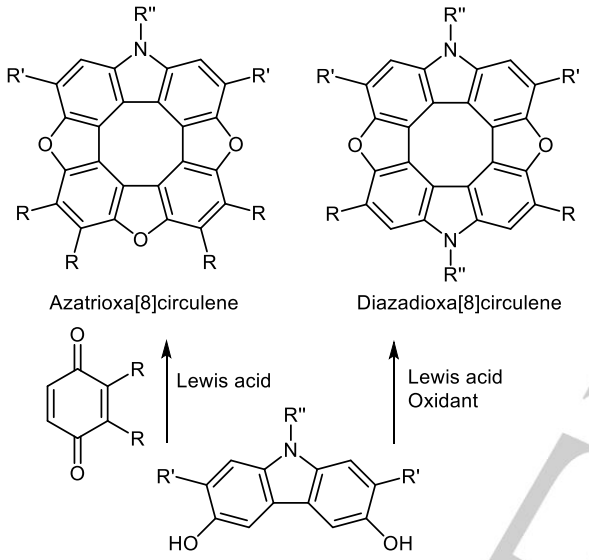

Figure 2. Generalized synthetic scheme for the synthesis of heterocyclic [8]circulenes using benzofurane scaffolding.

To further harness the attractive optical properties of azatrioxa[8]circulenes and the equally promising properties of PAHs we set out to to include anthracene moieties in the azatrioxa[8]circulenes. Herein we report on the synthesis of a dianthracenylazatrioxa[8]circulene. We characterize its spectroscopic properties, study its solvent-dependent fluorescence both experimentally and theoretically. Additionally, the crystal structure and charge hopping properties for the dianthracenylazatrioxa[8]circulene material are discussed. Finally, organic light-emitting diodes based on this novel compound as emissive layer were fabricated and characterized revealing the applicability of dianthracenylazatrioxa[8]circulene as a green emissive electroluminescent semiconductor.

Results and discussion

Synthesis

We have previously reported on the synthesis of azatrioxa[8]circulenes via the Lewis acid (BF_3•OEt_2) mediated tri-fold oxidative condensation between 3,6-dihydroxycarbazole **5** and either benzoquinone or naphthoquinone, to access **2** or **3**, respectively.[9b,c] In the present case using 1,4-anthraquinone **6** and **5** conveniently gave access to the target dianthracenylazatrioxa[8]circulene **4** (more details in ESI).

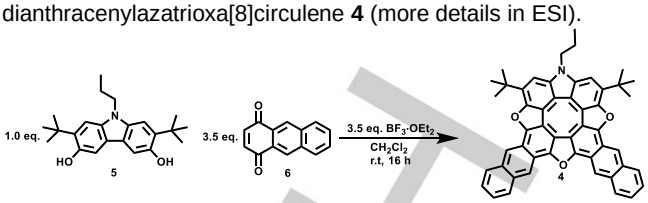

Scheme 1: Synthesis of the dianthracenylazatrioxa[8]circulene **4**. Isolated yield: 16%.

Single crystal X-ray structure

To further gain insight in the solid state structure of **4**, crystals suitable for SCXRD was readily obtained by slow evaporation of a solution of **4** in a mixture of CH_2Cl_2 and EtOH (Figure 3).

The azatrioxa[8]circulene **4** possesses cyclic 8π electron conjugation of the central COT and the structure is almost completely planar.The crystal structure also confirms the regiochemical outcome of the synthetic protocol. The crystal structure of **4** suggests there is little interaction between the π–systems of neighboring molecules (dimers A, B and C in Figure S1), probably due to a combination of the steric bulk of the two *tert*-butyl substituents on the azatrioxa[8]circulene structure and an attractive interaction between the anthracene moieties of one molecule and the circulene moiety of another molecule (dimers D and E in Figure S1). The crystal packing of the π-extended azatrioxa[8]circulene **4** is dominated by π stacking, with each azatrioxa[8]circulene exhibiting significant π–π overlap with its closest neighbor.

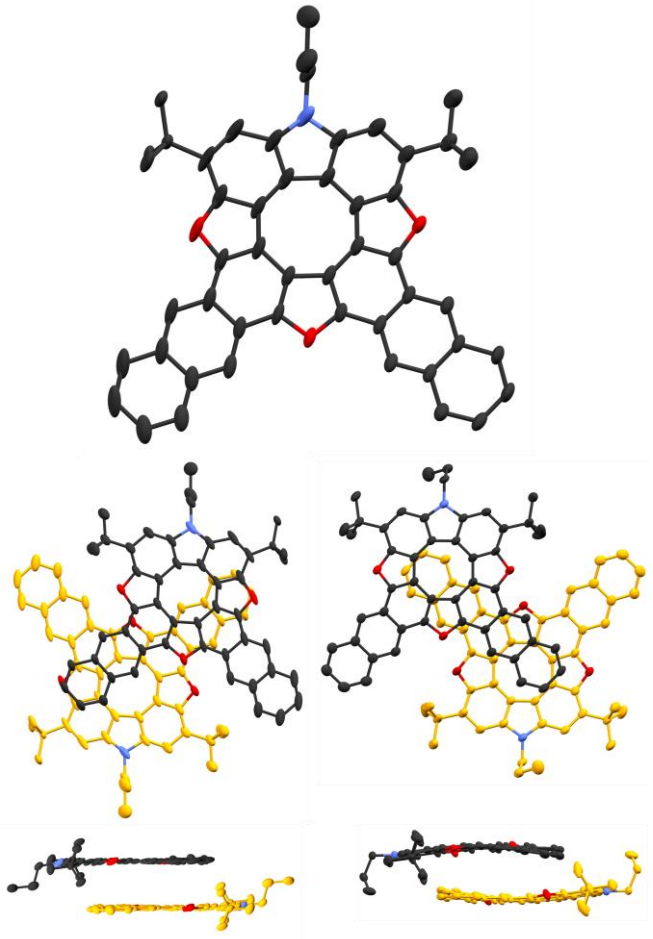

10.1002/chem.202100090

Figure 3. Single crystal X-ray structure of **4** with the stacked dimer highlighted. Hydrogen atoms are omitted for clarity. The C-C bond lengths in the central eight membered ring are all 1.4 (+/- 0.03) Å.

Electrochemical characterization

The redox properties of **4** were studied by cyclic voltammetry (CV) (Figure 4) and differential pulse voltammetry (DPV). Peak potentials, E_p, were recorded by CV, and formal potentials, E°′, were recorded. Circulene **4** is oxidized to the radical cation in a reversible one-electron process at E°′ = 0.32 V vs Fc/Fc^+, and further oxidation to a reactive dications are observed at E_p = 0.59 V and 0.83 V. By comparison, for the naphthalene-fused azatrioxa[8]circulene (**3**) the three oxidation waves are observed at the higher potentials (0.65, 1.22 and 1.65V).

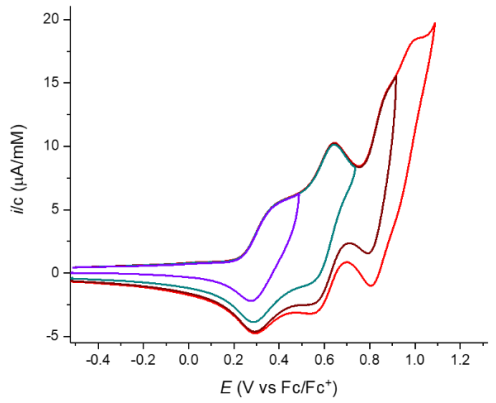

Figure 4. Cyclic voltammetry was carried out at 0.66 mM concentration of **4**. $(n\text{Bu})_4NPF_6$ (0.1 M) was used as supporting electrolyte. The working electrode was a circular glassy carbon disk (d = 3 mm). A Pt-wire served as the counter electrode and the reference electrode was Ag/Ag^+. The potential scale was subsequently calibrated by recording the potential of the ferrocene/ferrocenium redox couple. The voltage sweep rate was 0.1 V s^{-1} and all experiments were carried out at room temperature.

Aromaticity of dianthracenylazatrioxa[8]circulene

Compared to previously published reports on the aromaticity of hetero[8]circulenes,[12] dianthracenylazatrioxa[8]circulene **4** demonstrates a similar aromatic nature. Considerably positive NICS(0) and NICS(1) values confirm the presence of strong paratropicity (i.e. antiaromaticity) inside the inner eight-membered core, while all remaining five- and six-membered rings show negative values for the NICS(0) and NICS(1) indices implying the presence of a predominant diatropic ring current,i.e. aromaticity (Figure 5a).

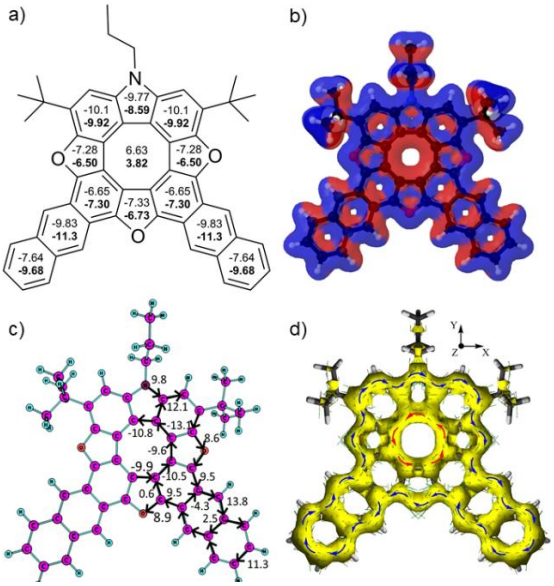

Figure 5. NICS(0) and NICS(1) (in bold) indices (a), the signed modulus of the MIC densities (b), MIC strengths vs. MIC pathway (c) and anisotropy of the induced current density plot (d) for the dianthracenylazatrioxa[8]circulene **4** molecule. Paratropic current densities are shown in red and the diatropic ones in blue in chart (b).

GIMIC calculations are in a complete agreement with the NICS indices. As can be seen from the magnetically induced current (MIC) density plots (Figure 5b) the inner eight-membered core indeed possesses a strong paratropic (anticlockwise) MIC, while the outer perimeter of dianthracenylazatrioxa[8]circulene sustains a diatropic (clockwise) MIC circulation. The MIC strength for paratropic and diatropic components was found to be similar in absolute values (−13.1 nA T^{-1} *vs.* 12.1 nA T^{-1}, respectively). The resulting MIC strength is only −1 nA T^{-1} meaning that **4** is globally non-aromatic. This feature can be interpreted in terms of "bifacial" aromaticity [12] which implies the existence of two self-cancelling MIC systems (paratropic in the inner eight-membered core, and diatropic along the outer perimeter). One should stress that the MIC strength along the radial CC bonds is very small (0.3-2.3 nA T^{-1}) in excellent agreement with the ACID plot (Figure 5d) which shows only a weak electron delocalization through these bonds (local currents in the benzene rings are quite weak). This fact indicates the presence of two weakly coupled MIC flows that circulate almost independently in opposite directions, i.e. "annulene-within-an-annulene" delocalization model of electron delocalization in compound **4** looks more preferable than a radialene model.

Optical and computational characterization

To further investigate the electronic structure of **4** attention was turned to optical UV/vis and fluorescence spectroscopy (Figure 6) in combination with TD-DFT calculations. The longest wavelength absorption maximum of **4** is located at 430 nm, similar to what has been reported for the smaller analogues (**2** and **3**) corroborating similar orbital nature of the corresponding electronic transitions. [8, 9b,c; 13] The absorption spectra of **4** are independent on solvent polarity and are in agreement with the TD-DFT calculations (Table S1, Figure S2). The first absorption band at 430 nm corresponds to the vertical electronic transition into the S_4 state (418 nm in CH_2Cl_2, *f*=0.323), while the S_0-S_1 (448 nm, *f*=0.0015), S_0-S_2 (432 nm, *f*=0.013) and S_0-S_3 (420 nm, *f*=0.014) transitions are predicted to be not sufficiently strong to produce individual absorption bands.

Focusing on the emissive properties of **4**, an interesting solvent-dependent fluorescence is observed for the lowest energy emission maxima: increasing the polarity of the hypsochromically shifts the lowest energy emission maxima.

Furthermore it has previously been reported [9c] that double benzannulation of **2**, to give **3**, gave an increase in fluorescence quantum yield (0.31 vs. 0.89, in CH_2Cl_2, respectively), this trend is clearly not continued in the series as the quantum yields of **4** are 0.17 in THF, 0.16 in CH_2Cl_2 and 0.27 in toluene. This can be explained in terms of charge-transfer character of S_1 state for circulene **4** (HOMO is localized on circulene macrocycle and anthracene branches, while LUMO localized only on anthracene branches). Therefore, the intensity of S_0-S_1 vertical absorption and S_1-S_0 vertical emission is considerably smaller than for

10.1002/chem.202100090

dinaphthylazatrioxa[8]circulene **3** for which both S_0-S_1 and S_1-S_0 transitions are very intensive.

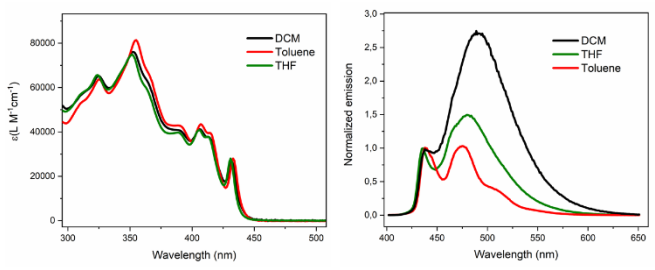

Figure 6: Absorption (a) and fluorescence (b) spectra of dianthracenylazatrioxa[8]circulene **4** (~10^{-5} M) measured in different solvents at room temperature.

Theoretical investigations indicate that the solvent-sensitive band (~475 nm) is a vibronic satellite of the main band at ~440 nm caused by the S_0-S_1 electronic transition. As follows from our quantum-chemical calculations, the Huang-Rhys factors (y_j) do not much depend on the nature of solvent (Table S2). The promotive modes 1426, 1653 and 1673 cm^{-1} (toluene as a model solvent) have the largest y_j values and accounting for Eq (2) (in ESI) the single excitation of these Franck-Condon active modes gives d_j^{FC}= 0.03, 0.02 and 0.02 a.u., respectively (the $< 0|\hat{d}|1 >$ transition dipole moment of the $S_0 \rightarrow S_1$ transition equals to 0.3 a.u.). The modes 1653 and 1673 cm^{-1} correspond to the stretching CC vibrations of the half part of inner eight-membered core, while the mode 1426 cm^{-1} corresponds to bending vibrations of the CH groups within the anthracene fragments (Figure S3). Other (but similar, Figure S4) vibrational modes are active in the Herzberg-Teller progression (Table S3) and the intensity of the corresponding vibronic transitions (d_j^{HT}) strongly depends on solvent polarity. It can be explained in terms of insensitivity of Huang-Rhys factors (y_j) on solvent nature, ω_j and the gradient V_j^f are independent on solvent, while the derivative of the transition dipole moment between the *i*-initial and *f*-final states depends on the solvent polarity within PCM model due to the asymmetrical displacement vectors of corresponding Q_j modes (Figure S4). As can be seen from Table 2 an additional vibrational mode 1667 cm^{-1} appears in the vibronic spectrum (d_j^{HT}=0.2) when considering the effect of the CH_2Cl_2 solvent within the PCM model. This fact explains the strong enhancement of the vibronic fluorescence band 475 nm in excellent agreement with the experimental spectra. For THF as a solvent, the Herzberg-Teller intensity of the vibronic transitions is approximately two times higher relative to toluene, but two times smaller than for THF. This computational prediction is in excellent agreement with the experimental observations (Figure 6). The excitation of low-frequency modes (in Herzberg-Teller approach) actually leads to the broadening of the vibronic spectrum that is also observed experimentally.

Mobility of charge carriers

As follows from our quantum-chemical calculations, the hole and electron reorganization energies for dianthracenylazatrioxa[8]circulene **4** are quite small and equals to 0.083 *eV* and 0.103 eV, respectively. Despite the smaller hole reorganization energy value dianthracenylazatrioxa[8]circulene **4** demonstrates a much higher electron mobility (2.258 $cm^2\ V^{-1}\ s^{-1}$ vs. 0.205 $cm^2\ V^{-1}\ s^{-1}$ for hole mobility). This is because of the more than four times higher value of the electron transfer integral (*V*) for the face-to-face π-stacked dimer **D** (Figure S1, Table S4).

One should note, that dianthracenylazatrioxa[8]circulene **4** is the best n-type semiconductor among other circulenes.[14] Thus, dianthracenylazatrioxa[8]circulene **4** can be considered as a promising organic ambipolar semiconductor (however, the n-type conductance dominates over the p-type one) that allows to use it in OLED heterostructures not only as an emissive material, but also as an hole/electron transporting material.

Dianthracenylazatrioxa[8]circulene as an emitter in OLEDs

Generally, derivatives of anthracene are well known materials for OLEDs.[15] They can play diverse role in OLEDs being emitting or transporting materials.[15c] Usually, the OLEDs based on anthracene derivatives demonstrate considerable triplet-triplet annihilation (TTA) effect that affect the external quantum efficiency of OLEDs higher than 5% which is a theoretical limit of fluorescent OLEDs.[15a,b] In case of dianthracenylazatrioxa[8]circulene 4 we do not observe any delayed fluorescence contributions, but due to the similarity in solid state arrangements with anthracene circulene 4 also demonstrate clear excimer emission both in photo- and electroluminescent spectra that is typical for anthracene derivatives.[16] Higher acenes like tetracene and pentacene are quite inefficient solid state emitters due to the high triplet yield through singlet fission and inter-system crossing[17]. However, some alkyl-substituted tetracene derivatives demonstrate extraordinary fluorescence quantum yield in solid state (up to 90%) due to the bulkiness and rigidity of the side alkyl group and the stacking pattern of neighboring molecules along the stacking direction. Obviously, the next step of our synthetic attempts would be the extension to tetracene- and pentacene-containing circulenes. This may help to increase a stability of teracene and pentacene fragments incorporated into the circulene framework against fast oxidation. At the same time, one can expect high charge carrier mobilities for tetracene- and pentacene-containing circulenes if they follow similar crystal packing in respect to teracene and pentacene single crystals.

The conventional electroluminescent structure of the device based on dianthracenylazatrioxa[8]circulene 4 emitter was fabricated by means of thermal vacuum evaporation of the organic compounds and metal electrodes onto the pre-cleaned ITO-coated (ITO = Indium Tin Oxide) glass substrates with a base pressure below 10^5Torr. The CuI which is amorphous and optically transparent highly conductive p-type semiconductor was used as a hole-injection layer in the conventional OLED scheme, while the TPBi layer (2,2′,2"-(1,3,5-benzinetriyl)-tris(1-phenyl-1-*H*-benzimidazole)) plays a double electron-transporting and hole-blocking function. For the inverted organic light-emitting diodes (IOLEDs), various efficient cathode structures can be realized. In this work we have used the n-type semiconductive zinc oxide (ZnO) deposited on pre-cleaned ITO by a spin-coating method [19]. One should stress, that the solution-processed ZnO film is widely used as an electron-injection layer in the IOLEDs.[20] The TPBi layer additionally supports the electron injection from the ZnO layer to the circulene emissive layer in IOLED and efficiently blocks the injection of holes at the same time. Except ZnO, the thermal vacuum evaporation has been used for the deposition of other functional layers upon IOLED fabrication following a step-by-step technique. Additionally, MoO_3 was used as a hole-injection layer [21] in the IOLED. Since Ca is highly reactive and corrodes quickly in an ambient atmosphere, Ca layer topped with an 200 nm of aluminium (Al) layer was used as the cathode in the

conventional OLED, while the pure Al layer was used as anode material in the IOLED. The active area of both obtained devices was 2*3 mm^2. The density-voltage and luminance–voltage dependences were recorded using a semiconductor parameter analyzer HP4145A. Measurement of brightness was obtained using a calibrated photodiode. Electroluminescence (EL) spectra were recorded with an Ocean Optics USB2000 spectrometer. The general composition of the two fabricated devises corresponds to the following scheme (Figure 7):

1) Conventional OLED: (An^+)ITO/CuI/**4**/TPBI/Ca/Al(Cat^-).

2) Inverted OLED: (Cat-)ITO/ZnO/TPBI/**4**/MoO_3/Al(An^+).

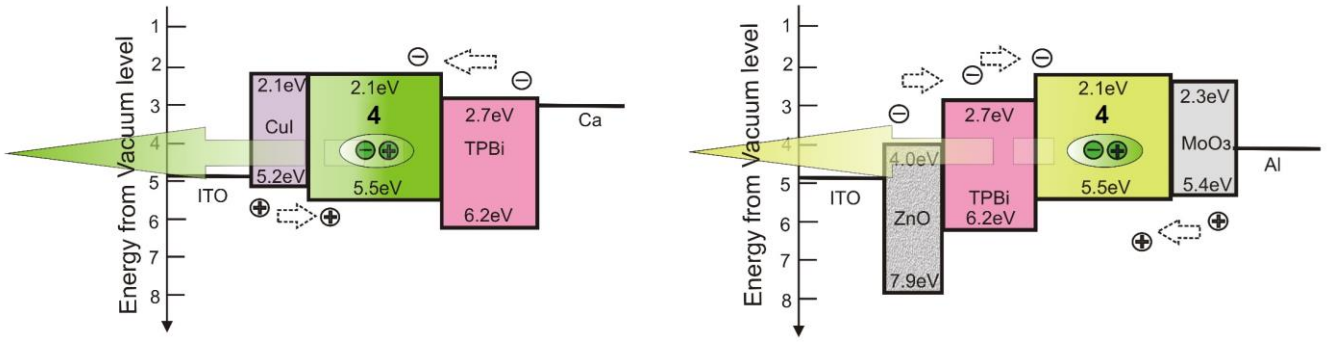

Figure 7. The energy diagrams of conventional (left) and inverted (right) OLEDs fabricated in this work.

Figure 8 represents a brightness characteristic and electroluminescence (EL) spectra of the conventional OLED structure. The short wavelength emission band (around 515 nm) in the photoluminescence (PL) spectrum of a solid-state film and in the EL spectrum of conventional OLED is caused by the singlet excitons recombination within the emissive layer of compound **4**. It seems that both PL and EL spectra in Figure 8 are red-shifted relative to the fluorescence spectra in solution and no clearly resolved vibronic structure is observed in the PL and EL spectra. This is most likely because of an aggregation behavior of circulene **4** which is supported by the clear presence of stacked dimers in crystal packing and also by the appearance of the low energy band in the PL and EL spectra (around 650 nm) caused by the excimer emission from stacked excited state dimers. However, there is a significant difference in ratios between the short (515 nm) and long (650 nm) wavelength band intensities observed in PL and EL spectra. This is attributed to single-molecule (i.e. localized) exciton emission pathway prevailing over the excimer channel due to the good electron-hole balance in the conventional OLED structure.

EL spectrum of the IOLED device is similar to the PL spectrum of the ZnO/**4** double-layer structure and also quite similar to the EL spectrum of the conventional OLED. Comparing all of them, one can observe the main emission band at around 515 nm and the weak band at 650 nm. However, a significant difference in the intensities of the long wavelength band at 650 nm is observed when comparing the PL spectra of the pure compound **4** film and the ZnO/**4** structure. The reason for the quenching of this excimer band in the complex ZnO/**4** film is most likely the energy transfer from the circulene to the ZnO layer that actually decreases the probability of excimer formation in the circulene film. The higher intensity of excimer emission under the influence of higher values of the applied bias in the inverted structure (comparing to the conventional one) comes from quadratic Stark effect similarly to previous reports.[22] The lighting characteristics of the conventional and inverted OLEDs based on the dianthracenylazatrioxa[8]circulene as an emitter are presented in the Table 1.

Table 1. Lightning characteristics of conventional and inverted OLEDs based on the dianthracenylazatrioxa[8]circulene emitter

Device	V_{on}, V		Current	Power	EQE,
		Max. brightness, cd m^{-2}	efficiency, cd A^{-1}	efficiency, lm W^{-1}	%
			at 100/max cd m^{-2}		
conventional	5.8	16 000	2.1/10.0	0.86/3.2	0.7/3.3
inverted	11.4	2800	1.5/3.0	0.3/0.5	0.5/1.1

One should stress, that the use circulene **4** as an emitter in the inverted scheme OLED is practically convenient for the future utilization of such IOLED in active-matrix OLED panels when the cathode of IOLED is turned on to the n-channel TFT (leakage) in the integrated circuit board with printed TFT.

Dianthracenylazatrioxa[8]circulene as a hole-transporting material in OLEDs

Accounting for the fact, that dianthracenylazatrioxa[8]circulene **4** can be considered as an ambipolar semiconductor, we have implemented it as a hole-transporting layer into an OLED based on the CdSeS/ZnS alloyed red-emissive quantum dots. The resulting device (so-called QLED) is composed as follows: ITO/CuI/ **4**/QD/$TSPO_1$/TPBI/Ca/Al (the energy diagram is presented in Figure 9). For this QLED both spin-coating and thermovacuum deposition techniques were used. At the first step, the organic heterostructure ITO/CuI/circulene was formed by means of a step-by-step thermal vacuum evaporation of layers. Secondly, the CdSeS/ZnS alloyed quantum dots were deposited on ITO/CuI/circulene **4** substrate by spin-coating technology. Finally, the hole blocking TSPO1 layer, electron transport TPBi layer and Ca/Al cathode were deposited by a thermovacuum evaporation technique. The resulting QLED is characterized by a clear red color electroluminescence. The EL maximum (630 nm) and FWHM of the EL spectrum (30 nm) are absolutely the same as those observed in photoluminescence spectra of CdSeS/ZnS alloyed quantum dots dissolved in toluene (λ_{em} = 630 nm, FWHM = 30 nm). The efficient transfer of charge carriers into the emissive layer supports the use of dianthracenylazatrioxa[8]circulene **4** as an appropriative hole-transporting material.

The lighting characteristics of the fabricated QLED are presented in a separate Table 2. The brightness 1600 cd m^{-2} and external quantum efficiency (EQE) 1.4% (Figure 9) were achieved for this device. As it can be seen from the QLED energy diagram (Figure 9), an edge of valence band (VB) of circulene **4** (5.5 eV) matches

well with the corresponding VB levels for the hole-injection CuI (5.2 eV) and emissive QD (6.0 eV) layers.

The usage of dianthracenylazatrioxa[8]circulene **4** as the hole-transporting layer makes it possible to smooth out the energy barrier for hole injection between CuI and QD layers and also to block the electron injection from the QD layer into the circulene conduction band (the energy barrier for such injection is around 2 eV) providing an electron-hole emissive recombination that takes place exclusively in the QD bulk.[23]

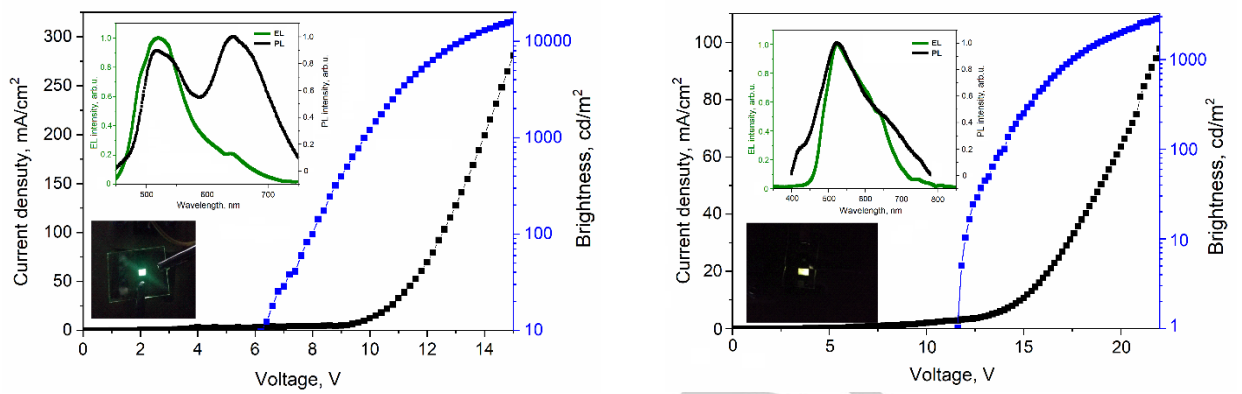

Figure 8. The current density/luminance vs. voltage characteristics of conventional (left) and inverted (right) OLEDs based on the dianthracenylazatrioxa[8]circulene emitter. The EL spectra of OLED vs. PL spectra of circulene **4** solid film (left) and ZnO/**4** heterostructure (right) are presented in insertions.

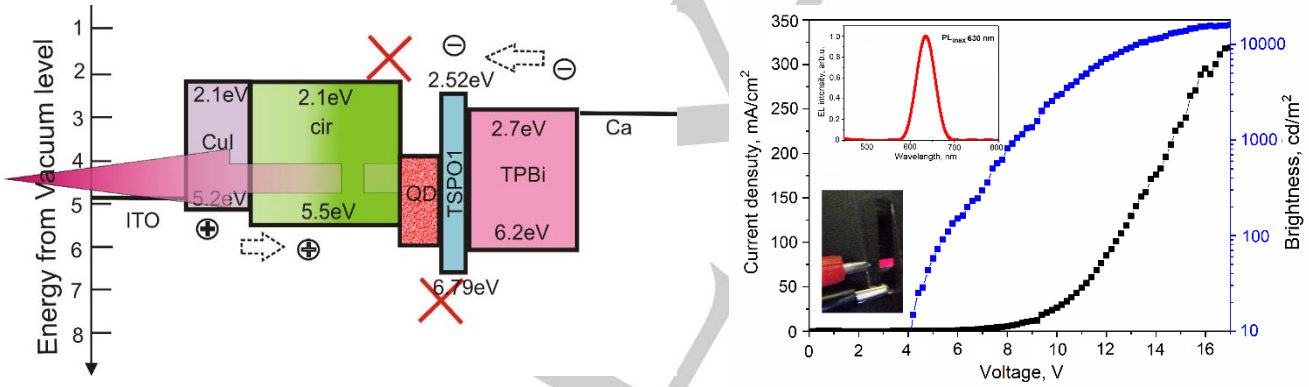

Figure 9. Energy diagram of the QLED fabricated in this work (top). The current density/luminance vs. voltage characteristics for the QLED including the EL spectrum of it (in the insertion) in comparison with the reference PL maximum for initial red-emissive CdSeS/ZnS alloyed quantum dots(bottom). Red cross denotes the energy barrier for charge carrier drift.

Table 2. Lightning characteristics of QLEDs based on the CdSeS/ZnS alloyed red-emissive quantum dots and dianthracenylazatrioxa[8]circulene hole-transporting material.

Device	V_{on}, V	Max. brightness, cd m^{-2}	Current efficiency, cd A^{-1}	Power efficiency, Lm W^{-1}	EQE, %
			at 100/max. cd m^{-2}		
QLED	4.0	1600	1.33/1.51	0.37/0.55	1.3/1.5

One should stress that the final lighting characteristics of the fabricated OLED are close to those published in the recent report by Nguyen *et. al.* [24] dedicated to technological surveys of appropriative conditions to achieve clear narrow electroluminescence from similar red-emissive CdSe/ZnS core/shell quantum dots.

Conclusions

We have presented the first time synthetic protocol and comprehensive structural, spectroscopic and theoretical characterization of the dianthracenylazatrioxa[8]circulene containing inner planar cyclooctatetraene core. As follows from the quantum-chemical calculations dianthracenylazatrioxa[8]circulene (similar to other previously published hetero[8]circulenes) contains two concentric flows of magnetically induced ring currents that circulate in opposite directions making the dianthracenylazatrioxa[8]circulene molecule non-aromatic as whole. The magnetically induced ring currents calculated along the radial CC bonds are very small as well as anisotropy of the induced current density assuming annulene-within-an-annulene model of π-delocalization for dianthracenylazatrioxa[8]circulene rather than radialene one. The solvent-dependent vibronic fluorescence spectra of dianthracenylazatrioxa[8]circulene is a distinct feature of this compound comparing to the related azatrioxa[8]circulene and dinaphthylazatrioxa[8]circulene. The close crystal packing of dianthracenylazatrioxa[8]circulene and the presence of π-stacked columns in the single crystal makes this material a promising ambipolar semiconductor that was confirmed by theoretical

calculations of charge carriers hopping rates (at the level of Marcus theory) and by implementing of dianthracenylazatrioxa[8]circulene into the organic light-emitting diodes (OLEDs) prototypes as emissive and hole-transporting material. The resulting lighting characteristics of OLEDs and variety of possible functions dianthracenylazatrioxa[8]circulene can play in OLEDs allows us to consider this new circulene as a promising material for organic electronics applications.

Acknowledgements

The research was carried out at the expense of the grant from Russian Science Foundation (project No. 17-73-20012). G. B. thanks for support to Swedish Research Council (grant No. 2020-04600) and to the Ministry of Education and Science of Ukraine (project no. 0121U107533). R. R. V. thanks for support to the Academy of Finland (grant number 1325369 and 1315600). The computations were enabled by resources provided by the Swedish National Infrastructure for Computing (SNIC) at the High Performance Computing Center North (HPC2N) partially funded by the Swedish Research Council through grant agreement no. 2018-05973. We acknowledge support from the Danish Council for Independent Research (DFF4181-00206 and 9040-00265), from Carlsbergfondet (CF18-0149) and from the University of Copenhagen.

Keywords: Circulene • OLED • PAH • Synthesis • Anthracene

[1] a) J. Lee, C. Chen, P. Lee, H. Lin, M. Leung, T. Chiu, C. Lin, *J. Mater. Chem. C* **2019**, 7, 5874-5888; b) D. Ma, Z. Xu, B. Z. Tang, Y. Wang, *J. Mater. Chem. C* **2020**, 8, 2614-2642; c) Y. Li, J-Y. Liu, Y.-D. Zhao, Y.-C. Cao, *Mater. Today* **2017**, 20, 258-266.

[2] a) L. Yu, Z. Wu, G. xie, W. Zeng, D. Ma and C. Yang, *Chem. Sci.* **2018**, 9, 1385-1391; b) Z. Huang, Z. Bin, R. Su, F. Yang, J. Lan, J. You, *Angew. Chem. Int. Ed.* **2020**, 59, 9992-9996; c) Y. Im, M. Kim, Y. J. Cho, J.-A. Seo, K. S. Yook, J. Y. Lee, *Chem. Mater.* **2017**, 29, 1946-1963.

[3] a) B. Wex, B. R. Kaafarani, *J. Mater. Chem. C* **2017**, 5, 8622-8653; b) M. Reig, C. Gozalvez, R. Bujaldon, G. Bagdziunas, K. Ivaniuk, N. Kostiv, D. Volyniuk, J. V. Grazulevicius, D. Velasco, *Dyes Pigm.* **2017**, 137, 24-35; c) D. Volyniuk, V. Cherpak, P. Stakhira, B. Minaev, G. Baryshnikov, M. Chapran, A. Tomkeviciene, J. Keruckas, J. V. Grazulevicius, *J. Phys. Chem. C* **2013**, 117, 22538−22544.

[4] R. R. Valiev, R. M. Gadirov, K. M. Degtyarenko, D. V. Grigoryev , R. T. Nasubullin, G. V. Baryshnikov, B. F. Minaev, S. K. Pedersen, M. Pittelkow, *Chem. Phys. Lett.* **2019**, 732, 136667-136671.

[5] a) T. Hensel, N. N. Andersen, M. Plesner, M. Pittelkow, *Synlett.* **2016**, 27, 498-525; b) Y. Miyake, H. Shinokubo, *Chem. Commun.*, **2020**, 56, 15605-15614; c) N. N. Karaush, G. V. Baryshnikov, V. A. Minaeva, H. Ågren, B. F. Minaev, *Mol. Phys.* **2017**, 115, 2218-2230; d) G. V. Baryshnikov, B. F. Minaev, V. A. Minaeva, *Russ. Chem. Rev.* **2015**, 84 455-484.

[6] a) N. N. Karaush, G. V. Baryshnikov, H. Ågren, B. F. Minaev, *New J. Chem.* **2018**, 42, 11493-11505; b) N. N. Karaush-Karmazin, G. V. Baryshnikov, L. I. Valiulina, R. Valiev, H. Ågren, B. F. Minaev, *New J. Chem.* **2019**, 43, 12178-12190.

[7] J. H. Dopper, H. Wynberg, *J. Org. Chem.* **1975**, 40, 1957-1966.

[8] G. V. Baryshnikov, R. R. Valiev, N. N. Karaush, V. A. Minaeva, A. N. Sinelnikov, S. K. Pedersen, M. Pittelkow, B. F. Minaev, H. Ågren, *Phys. Chem. Chem. Phys.* **2016**, 18, 28040-28051.

[9] a) C.B. Nielsen, T. Brock-Nannestad, T. K. Reenberg, P. Hammershøj, J. B. Christensen, J.W. Stouwdam, M. Pittelkow, *Chem. Eur. J.* **2010**, 16, 13030-13034; b) C. B. Nielsen, T. Brock-Nannestad, P. Hammershøj, T. K. Reenberg, M. Schau-Magnussen, D. Trpcevski, T. Hensel, R. Salcedo, G. V. Baryshnikov, B. F. Minaev, M. Pittelkow, *Chem. Eur. J.* **2013**, 19, 3898-3904; c) T. Hensel, D. Trpcevski, C. Lind, R. Grosjean, P. Hammershøj, C. B. Nielsen, T. Brock-Nannestad, B. E. Nielsen, M. Schau-Magnussen, B. Minaev, G. V. Baryshnikov, M. Pittelkow, *Chem. Eur. J.* **2013**, 19, 17097-17102.

[10] K. Ivaniuk, G. Baryshnikov, P. Y. Stakhira, S. Pedersen, M. Pittelkow, A. Lazauskas, D. Y. Volyniuk, J. V. Grazulevicius, B. Minaev, H. Ågren, *J. Mater. Chem. C* **2017**, 5, 4123-4128.

[11] a) H. Erdtman, H.-E. Högberg, *Chem. Commun*. **1968**, 773-774; b) H. Erdtman, H.-E. Högberg, *Tetrahedron Lett.* **1970**, 3389-3392.

[12] a) S. Radenkovic, I. Gutman, P. Bultinck, *J. Phys. Chem. A* **2012**, 116, 9421-9430; b) G. V. Baryshnikov, B. F. Minaev, M. Pittelkow, C. B. Nielsen, R. Salcedo, *J. Mol. Model.* **2013**, 19, 847-850; c) G. V. Baryshnikov, R. R. Valiev, N. N. Karaush, B. F. Minaev, Phys. Chem. Chem. Phys. 2014, 16, 15367-15374; d) G. V. Baryshnikov, N. N. Karaush, B. F. Minaev, *Chem. Heterocycl. Comp.* **2014**, 50, 349-363; e) G. V. Baryshnikov, N. N. Karaush, R. R. Valiev, B. F. Minaev, *J. Mol. Mod.* **2015**, 21, 136-144; f) G. V. Baryshnikov, R. R. Valiev, N. N. Karaush, D. Sundholm, B. F. Minaev, *Phys. Chem. Chem. Phys.* **2016**, 18, 8980-8992; g) G. V. Baryshnikov, R. R. Valiev, V. N. Cherepanov, N. N. Karaush-Karmazin, V. A. Minaeva, B. F. Minaev, H. Ågren, *Phys. Chem. Chem. Phys.* **2019**, 21, 9246−9254; h) S. K. Pedersen, K. Eriksen, H. Ågren, B. F. Minaev, N. N. Karaush-Karmazin, O. Hammerich, G. V. Baryshnikov, Michael Pittelkow, *J. Am. Chem. Soc.* **2020**, 142, 14058-14063; i) B. Lousen, S. K. Pedersen, P. Bols, K. H. Hansen, M. R. Pedersen, O. Hammerich, S. Bondarchuk, B. Minaev, G. V. Baryshnikov, H. Ågren, M. Pittelkow, *Chem.-Eur. J.* **2020**, 26, 4935−4940.

[13] a) B. F. Minaev, G. V. Baryshnikov, V. A. Minaeva, *Comput. Theor. Chem.* **2011**, 972, 68–74; b) N. N. Karaush, B. F. Minaev, G. V. Baryshnikov, V. A. Minaeva, *Opt. Spectrosc.* **2014**, 116, 33-46; c)

[14] a) N. N. Karaush-Karmazin, G. Baryshnikov, A. Kuklin, D. Saykova, H. Ågren, B. Minaev, *J. Mater. Chem. C* **2020**, doi.10.1039/D0TC03674A; b) J. Yin, C. Kadali, X.-H. Ju, *J. Mater.Chem. C* **2015**, 3, 3472-3481; c) T. Fujimoto, R. Suizu, H. Yoshikawa, K. Awaga, *Chem.-Eur. J.* **2008**, 14, 6053-6056; d) G. Gahungu, J. Zhang, T. Barancira, *J. Phys. Chem. A* **2009**, 113, 255-262; e) S. Mohakud, S. K. Pati, *J. Mater. Chem.* **2009**, 19, 4356-4361; f) X.-D. Tang, Y. Liao, H.-Z.Gao, Y.Geng, Z.-M. Su, *J. Mater. Chem.* **2012**, 22, 6907–6918.

[15] a) M. Aydemir, G. Haykır, A. Battal, V. Jankus, S. K. Sugunan, F. B. Dias, H. Al-Attar, F. Türksoy, M. Tavaslı, A. P. Monkman, *Organ. Electron.* **2016**, 30, 149-157. b) H. Fukagawa, T. Shimizu, N. Ohbe, S. Tokito, K. Tokumaru, H. Fujikake, Organ. Electron. **2012**, 13, 1197-1203. c) J. Huang, J.-H. Sua, H. Tian, *J. Mater. Chem.* **2012**, 22, 10977-10989.

[16] a) C. Zhao, X. Cai, Z. Ma, J. Shi, L. Xu, H. Wang, *J. Photochem. Photobiol. A*, **2018**, 355, 318-325. b) Y. Gao, H. Liu, S. Zhang, Q. Gu, Y. Shen, Y. Ge, B. Yang, *Phys. Chem. Chem. Phys.* **2018**, 20, 12129-12137. c) F. Huanga, G. Feng, *RSC Adv.* **2014**, 4, 484-487.

[17] a) J. J. Burdett, A. M. Müller, D. Gosztola, C. J. Bardeen, *J. Chem. Phys.* **2010**, 133, 144506. b) C. Kryschi, H.-C. Fleischhauer, B. Wagner, *Chem. Phys.* **1992**, *161*, 485-491.

[18] C. Kitamura, *Chem. Rec.* **2012**, *12*, 506-514.

[19] M. Shibata, Y. Sakai, D. Yokoyama, *J. Mater. Chem. C*, **2015**, 3, 11178-11191.

[20] a) G. Shi, X. Zhang, M. Wan, S. Wang, H. Lian, R. Xua, W. Zhu, *RSC Adv.* **2019**, 9, 6042-6047; b) Y. Chen, S. Chu, R. Li, Y. Qin, Y. Xu, X. Zhang, J. Wang, M. Liu, W.-Y. Lai, W. Huang, *Org. Electron.* **2019**, 66, 1–6.

[21] a) J. W. Ma, Z. Liang, C. Jina, X. Y. Jiang, Z. L. Zhang, *Solid State Commun.* **2009**, 149, 214-217; b) H. Zhang, Q. Fu, W. Zeng, D. Ma, *J. Mater. Chem. C* **2014**, 2, 9620-9624.

[22] a) M. Koch, M. Myahkostupov, D. G. Oblinsky, S. Wang, S. Garakyaraghi, F. N. Castellano, G. D. Scholes, *J. Am. Chem. Soc.* **2017**, 139, 5530-5537; b) G. Candiotto, R. Giro, B. A. C. Horta, F. P. Rosselli, M. de Cicco, C. A. Achete, M. Cremona, R. B. Capaz, *Phys. Rev. B* **2020**, 102, 235401-235407.

[23] a) A. Fokina, Y. Lee, J. H. Chang, M. Park, Y. Sung, W. K. Bae, K. Char, C. Lee, R. Zentel, *Adv. Mater. Interfaces* **2016**, 3, 1600279-1600287; b) Q. Huang, J. Pan, Y. Zhang, J. Chen, Z. Tao, C. He, K. Zhou, Y. Tu, W.

Lei, *Opt. Express* **2016**, 24, 25955-25963; c) K. Sun, F. Li, Q. Zeng, H. Hu, T. Guo, *Org. Electron.* **2018**, 63, 65–70.
[24] T. C. Nguyen, T. T. T. Can, W.-S. Choi, *Sci. Rep.* **2019**, 9, 13885-13893.

10.1002/chem.202100090

WILEY-VCH

COMMUNICATION

Entry for the Table of Contents

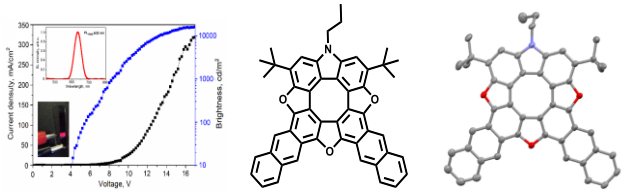

A π-extended fully conjugated antiaromatic azatrioxa[8]circulene–PAH structure is prepared, fully characterized and utilized in as the emitter in brightly emitting OLEDs, IOLEDs and QLEDs.